Electronic Supplementary Material (ESI) for Materials Horizons.

Electronic Supporting Information for the manuscript:

A magnetocaloric composite based on molecular coolers and carbon nanotubes with enhanced thermal conductivity

Olivier Roubeau, Eva Natividad, Marco Evangelisti, Giulia Lorusso, Elías Palacios

Table of contents

Figure S1. TEM images of raw MWCNTs p. 2
Figure S2. Thermogravimetric analysis data p. 3
Figure S3. Powder X-ray diffractograms of MWCNT-ox and MWCNT-[Gd_2ac] p. 4
Figure S4. XPS spectra of MWCNT-ox: survey and O 1S region p. 5
Figure S5. XPS spectra of MWCNT-ox: C 1S and Gd 3d and 4 d regions p. 6
Figure S6. Infra-red spectra of [Gd_2ac] and MWCNT-[Gd_2ac] p. 8
Figure S7. Infra-red spectra of [Gd_2ac] and physical mixture of MWCNT-ox and [Gd_2ac] p. 9
Figure S8. Raman spectra of MWCNT-ox and MWCNT-[Gd_2ac] p. 10
Figure S9. Powder X-ray diffractogram of the TGA residue of MWCNT-[Gd_2ac] p. 11
Figure S10. Comparison of thermogravimetric analysis of [Gd_2ac] and MWCNT-[Gd_2ac] p. 12
Table S1. Details and interpretation of thermogravimetric analysis results p. 13
Figure S11. Magnetization of the [Gd_2ac] content in the composite material p. 14
Figure S12. Magnetic entropy change of the [Gd_2ac] content in the composite material p. 15
Figure S13. Heat capacity of bulk-[Gd_2ac] p. 16
Figure S14. Thermal conductivity of the LR White resin p. 17
Figure S15. Thermal conductance set-up and samples p. 18
Table S2. Dimensions, weights and apparent densities of thermal conductivity samples p. 19
Figure S16. Direct MCE measurement for a m = 0.81 mg sample of bulk-[Gd_2ac] p. 20
Figure S17. Direct MCE measurement for a m = 8.1 mg sample of bulk-[Gd_2ac] p. 21
Figure S18. Direct MCE measurement for an array of parallel buckypapers of MWCNT-[Gd_2ac] p. 22
Modelling of thermal conductivity for the direct MCE measurements p. 23

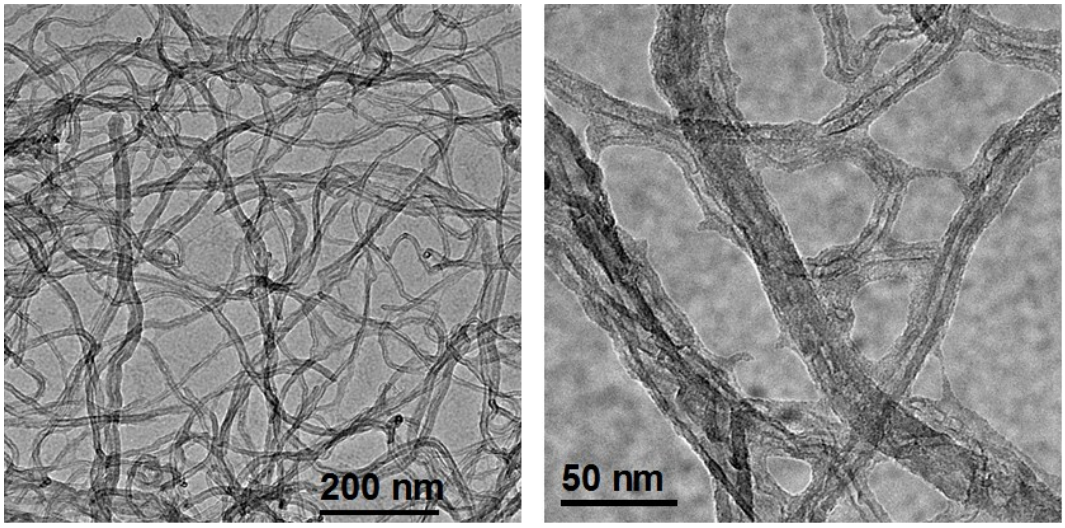

Figure S1. TEM images of the used raw MWCNTs after dispersion in water with sodium dodecyl sulphate and tip sonication.

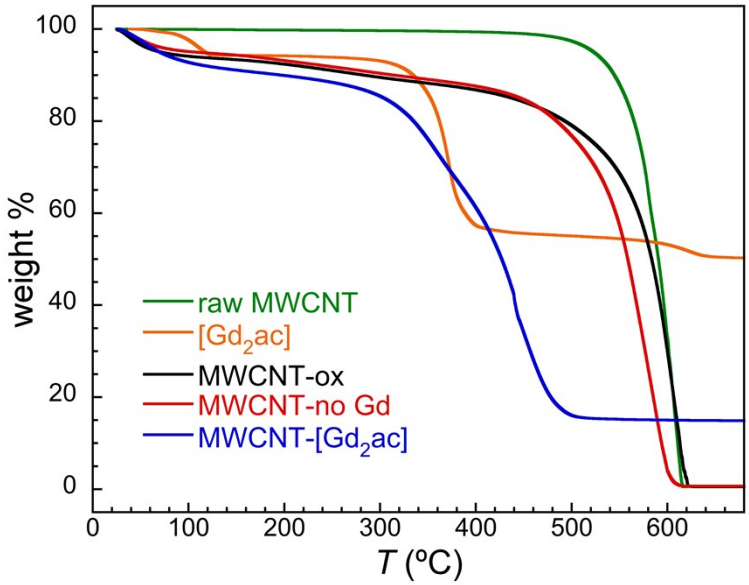

Figure S2. Thermogravimetric analysis under synthetic air performed at 10º/min on the indicated materials.

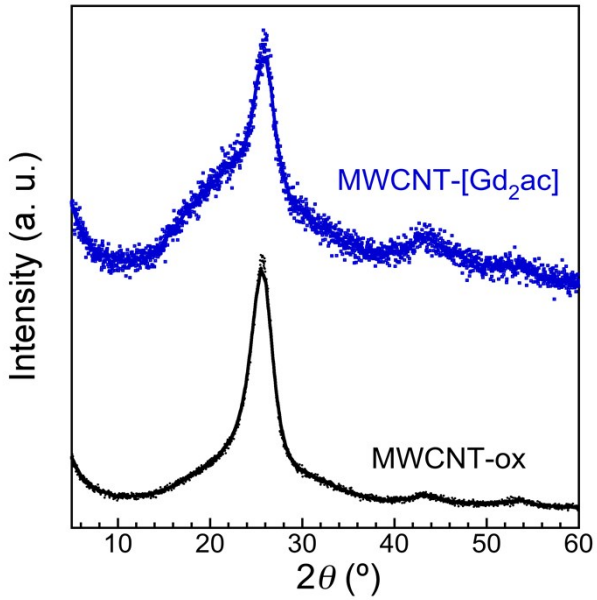

Figure S3. Powder X-ray diffractograms of bucky papers of MWCNT-ox and MWCNT-[Gd_2ac], dominated by the peak at *ca.* 25.8º characteristic of the 002 reflection from the graphitic layer structure of MWCNT, and corresponding to the inter-wall separation of *ca.* 3.4 Å. Full lines are weighted smoothing of the experimental data (symbols).

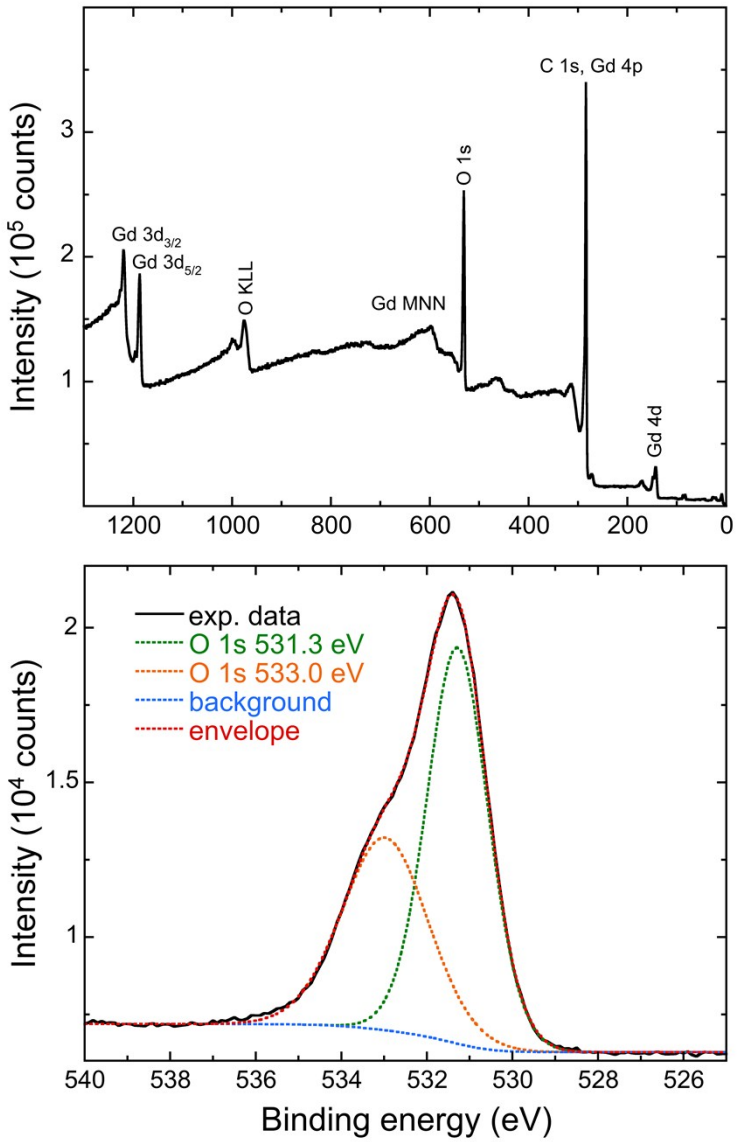

Figure S4. X-ray Photoelectron Spectroscopy (XPS) data for MWCNT-[Gd_2ac]. Top: survey spectrum with relevant peak assignment indicating the presence of Gd, C and O. Bottom: high resolution spectrum of the O 1S region and its simulation with two components (Gaussian-Lorentzian) and background (Shirley), as indicated.

The peak at 531.3 eV (FWHM = 1.7 eV, area = 23444 eV-cts/s, 59.6 %) can be ascribed to O from carbonyl groups of protonated carboxylic groups and O from deprotonated coordinated carboxylic groups.[1] The peak at 533.0 eV (FWHM = 2.3 eV, area = 15897 eV-cts/s, 40.4 %) would then correspond to O in hydroxyl groups of protonated carboxylic groups, water and other less oxidised functions on the oxidised MWCNT component. Most importantly, the absence of any peak/shoulder at lower binding energies precludes the presence of any Gd_2O_3 in the MWCNT-[Gd_2ac] composite.[2]

[1] J. V. Barth et al., *Small* **2015**, 11, 6358-6364

[2] Lattice oxygen in Gd_2O_3 is expected at *ca.* 529.0 eV, see A. Gasparotto et al. *Surf. Sci. Spectra* **2007**, 14, doi: 10.1116/11.20080703

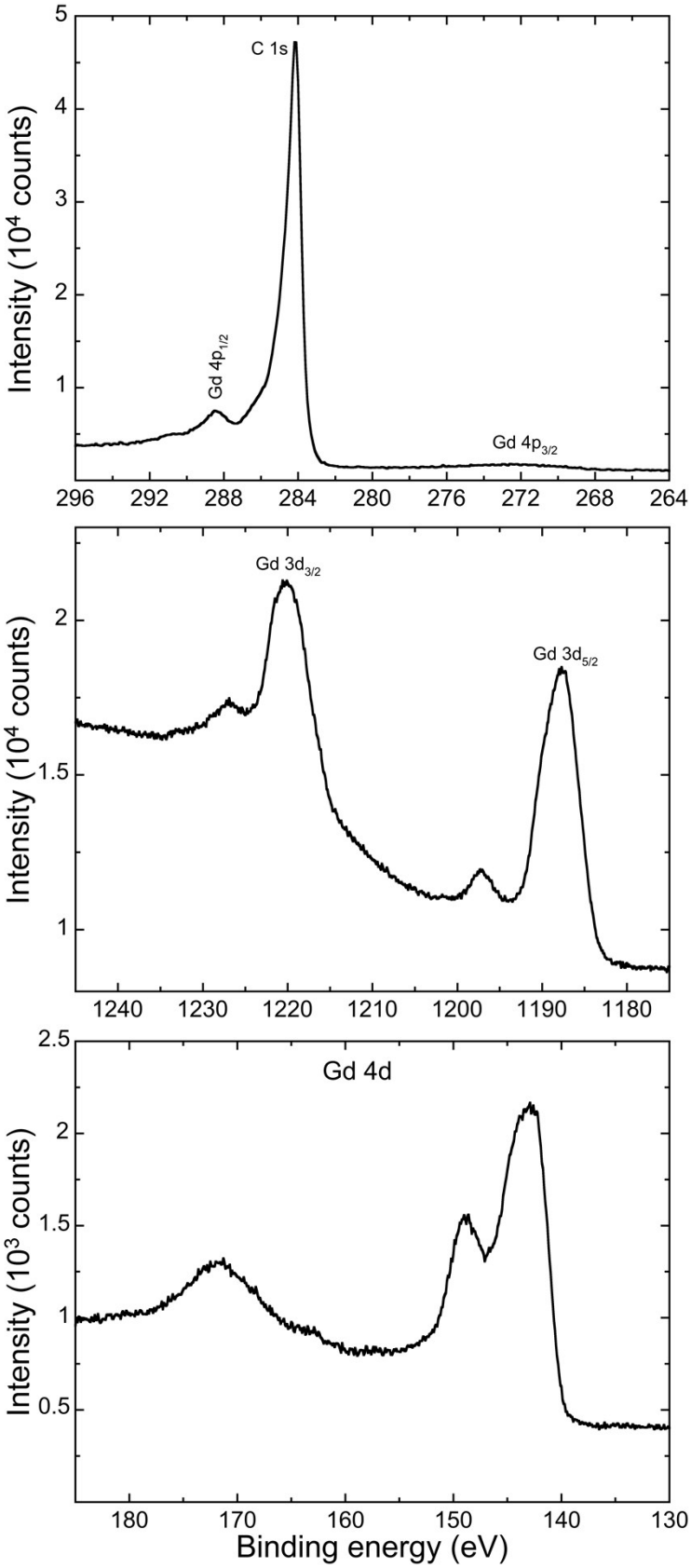

Figure S5. X-ray Photoelectron Spectroscopy (XPS) of MWCNT-[Gd_2ac]. High resolution spectra of the C 1S and Gd 4p region (top), the Gd 3d region (middle) and the Gd 4d region (bottom).

The C 1s peak is typical of oxidized MWCNTs with one main component corresponding to the graphite-like core (284.2 eV) and a broad shoulder at higher binding energies corresponding to C at various degrees of oxidation, including carboxylic groups. The Gd $4p_{1/2}$ peak appears at the end of this shoulder (288.4 eV) and the broad Gd $4p_{1/2}$ is at *ca.* 272.5 eV.
The Gd 3d spectrum has two main peaks corresponding to the Gd $3d_{3/2}$ (1220.1 eV) and the Gd $3d_{5/2}$ (1187.8 eV), in addition to two shake-up peaks (1227.1 and 1197.2 eV). These binding energies, and in particular that of the Gd $3d_{5/2}$ are consistent with Gd in a +3 oxidation state.[1,2]
The Gd 4d spectrum shows a multiplet structure, with one main peak at 143.0 eV, a second weaker peak at 148.8 eV, and a broad satellite ca. 30 eV above the main peak (171.8 eV). This complex spectrum likely arises from the electrostatic interactions between the 4d hole and 4f electrons, significant due to the same principal quantum number of both shells.[2] The spectrum is again consistent with Gd in a +3 oxidation state as in Gd_2O_3.[2]

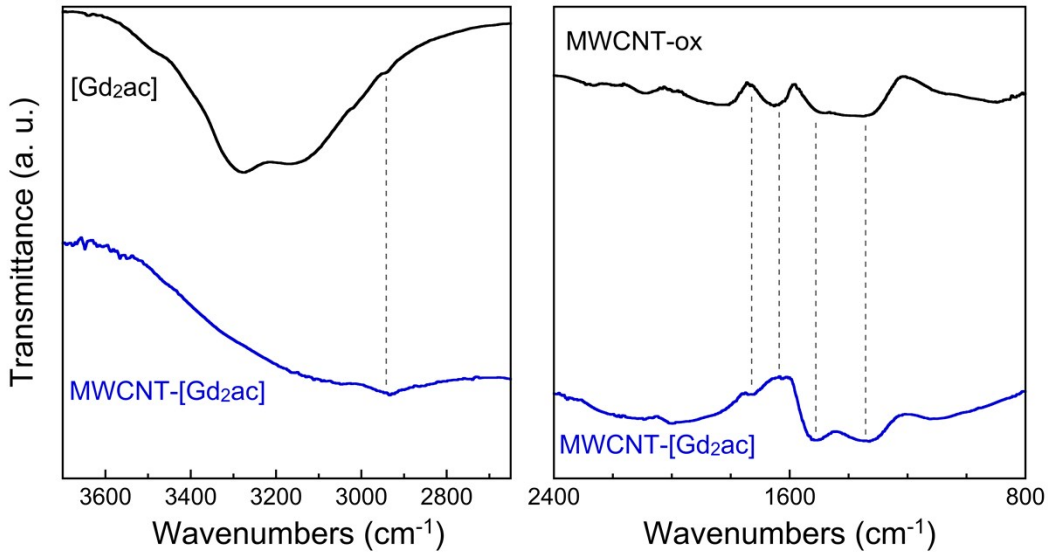

Figure S6. Infra-red spectra of [Gd_2ac] and MWCNT-[Gd_2ac]. Vertical dashed lines highlight common features.

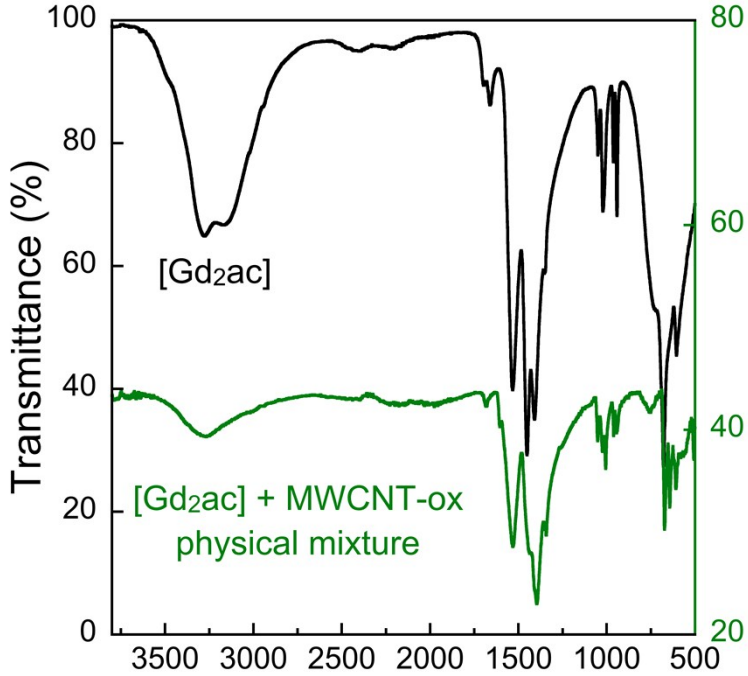

Figure S7. Infra-red spectra of [Gd_2ac] and a physical mixture of MWCNT-ox and [Gd_2ac].

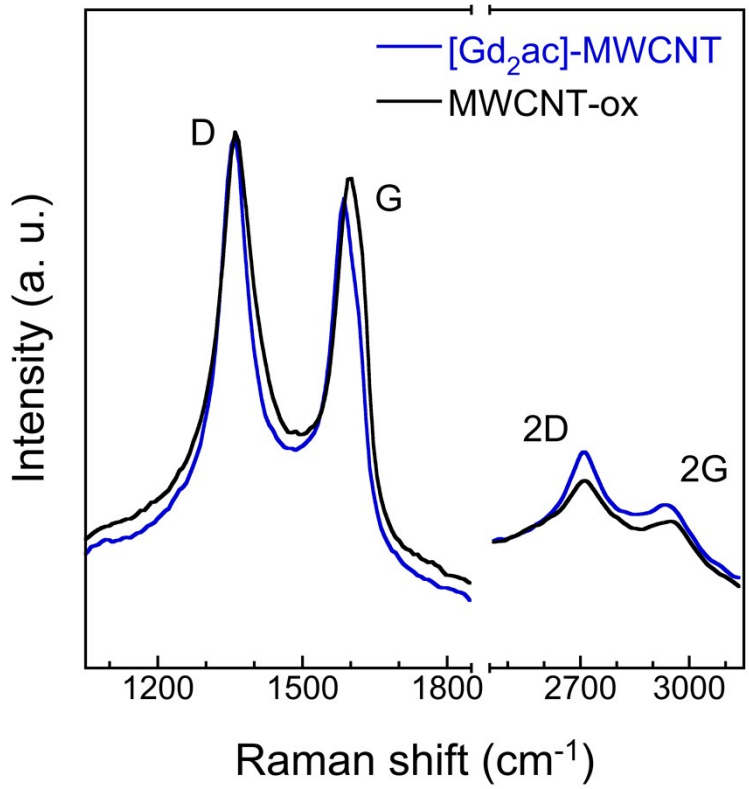

Figure S8. Raman spectra of MWCNT-ox and MWCNT-[Gd_2ac].

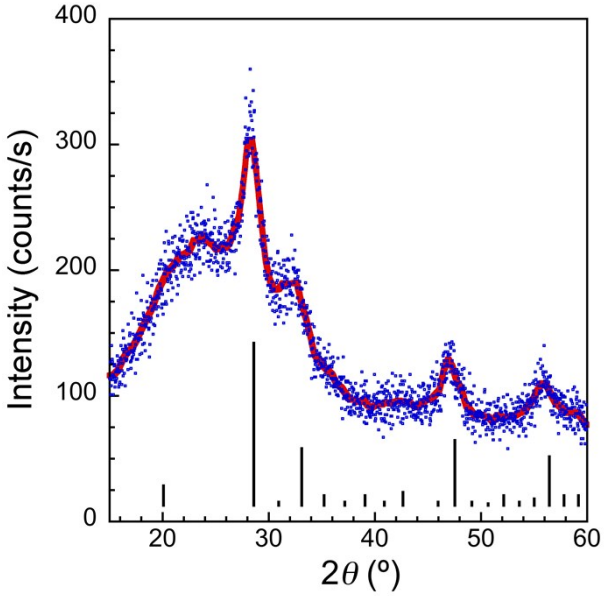

Figure S9. Powder X-ray diffractogram of the whitish residue after thermogravimetric analysis under synthetic air up to 700 ºC of MWCNT-[Gd_2ac]. The full line is a weighted smoothing of the experimental data (symbols). Vertical bars represent the reflections of the cubic form of Gd_2O_3 (JCPDS 12-0797), the height being proportional to their relative intensity.

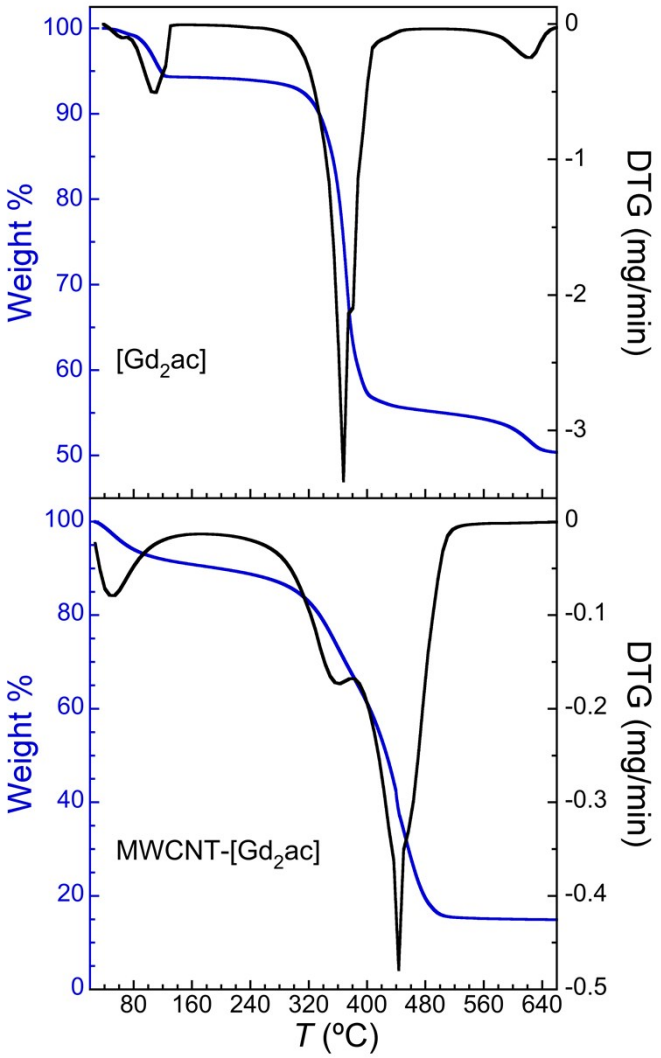

Figure S10. Comparison of the weight loss and its time derivative observed during thermogravimetric analysis under synthetic air for [Gd_2ac] (top) and MWCNT-[Gd_2ac] (bottom).

Table S1. Details and interpretation of thermogravimetric analysis results for raw MWCNT, MWCNT-ox, unreacted MWCNT-ox, MWCNT-[Gd_2ac] and [Gd_2ac].

Sample	weight % (*T* in ºC)	weight loss (%)	*T* range (ºC)	T^{peak} (ºC)	Interpretation weight loss
raw MWCNT	99.4 (330)	0.6	30-400	-	moist + defects
	0.5 (620)	98.1	400-620	605	oxidation CNT
MWCNT-ox	93.0 (150)	7.0	30-150	-	water
	87.1 (390)	5.9	150-390	265	oxygen-rich functions
	0.5 (630)	86.6	390-630	607	oxidation CNT
unreacted MWCNT-ox	94.3 (150)	5.7	30-150	-	water
	87.9 (390)	6.4	150-390	265	oxygen-rich functions
	0.6 (630)	87.3	390-630	590	oxidation CNT
MWCNT-[Gd_2ac]	89.6 (210)	10.4	30-210	-	water
	61.9 (400)	27.7	210-400	362	acetate to carbonate [Gd_2ac] + O-rich functions on CNT
	15.2 (550)	26.7	400-550	443	oxidation CNT + oxidation to Gd_2O_3
[Gd_2ac]	94.3 (130)	5.7	30-130	107	water
	55.7 (440)	38.6	130-440	368	acetate to carbonate
	50.4 (660)	5.3	440-660	625	oxidation to Gd_2O_3

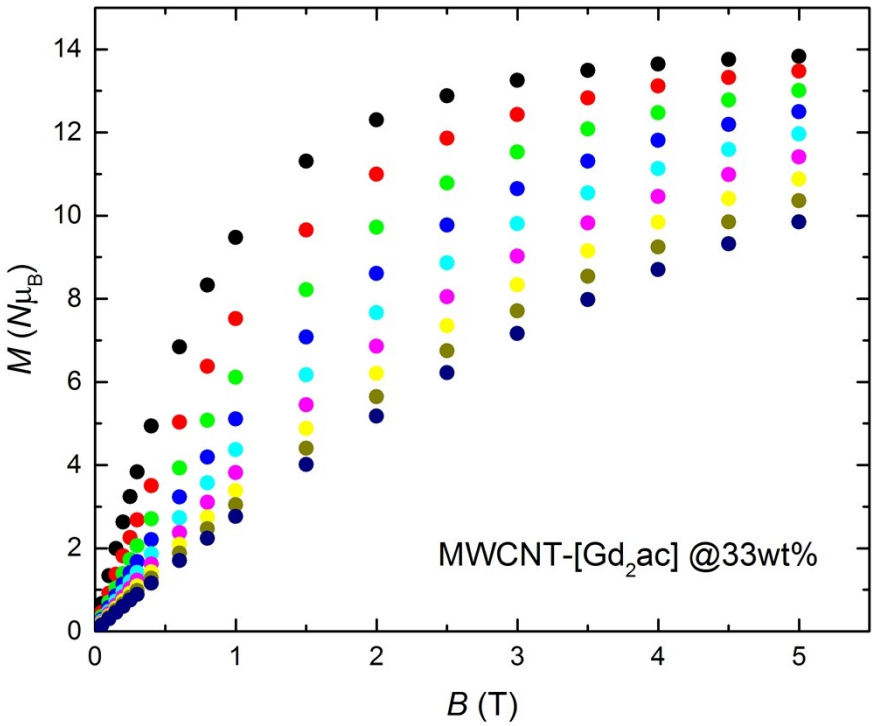

Figure S11. Magnetization of the [Gd_2ac] content in the composite material MWCNT-[Gd_2ac] vs. applied field for temperatures from 2 K (black dots) to 10 K (dark blue dots), in 1 K steps.

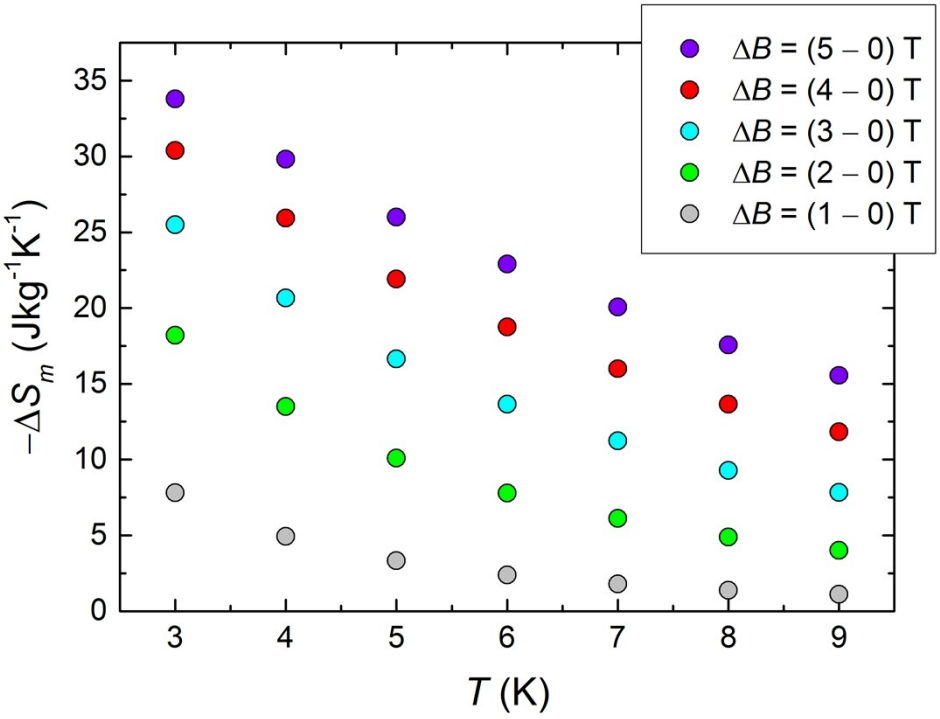

Figure S12. Temperature dependence of the magnetic entropy change $\Delta S_m(T,\Delta B)$ at the indicated applied field-changes ΔB, as derived indirectly from magnetization data (Figure S9).

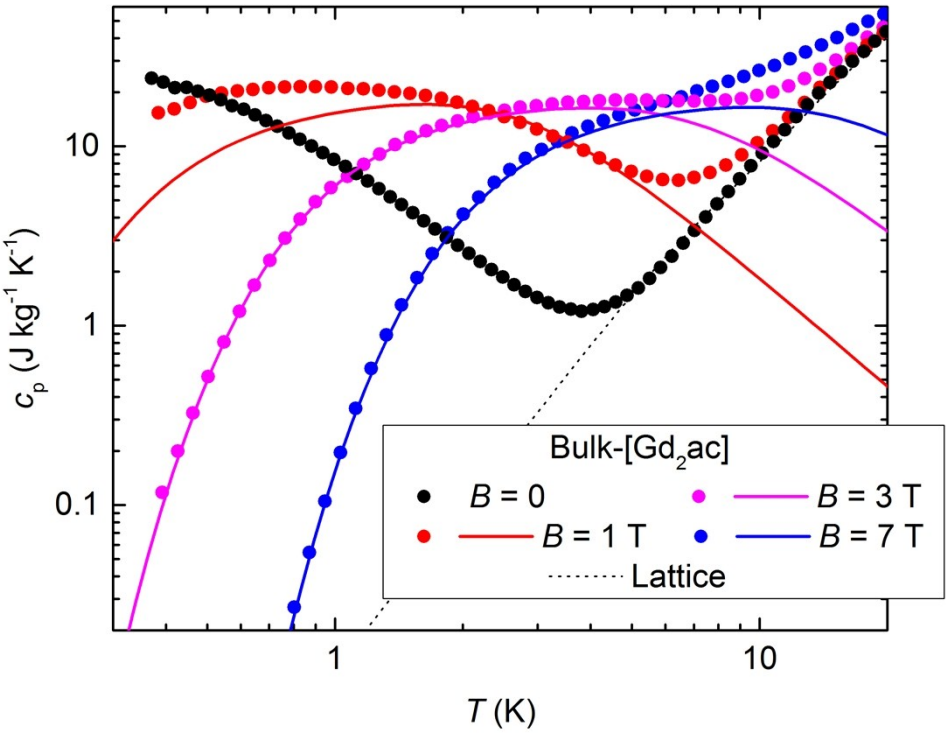

Figure S13. Temperature-dependence of the mass heat capacity of bulk-[Gd_2ac], for selected applied field values, as labeled. Solid lines are the Schottky heat capacities for J = 0.07 K (see text), while dashed line is the lattice contribution to the heat capacity.

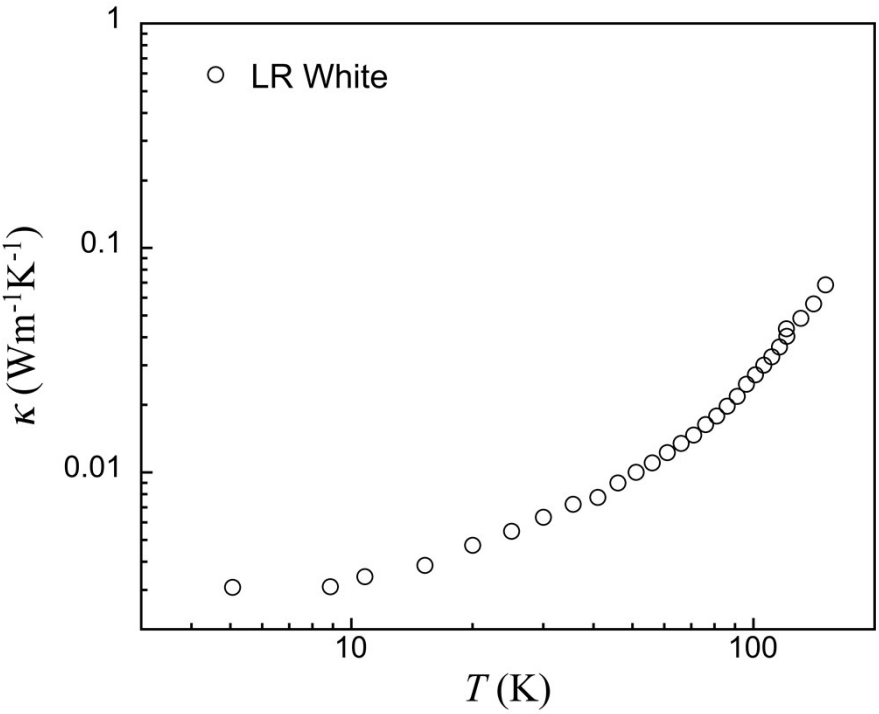

Figure S14. Thermal conductivity of the LR White acrylic resin for electron microscopy.

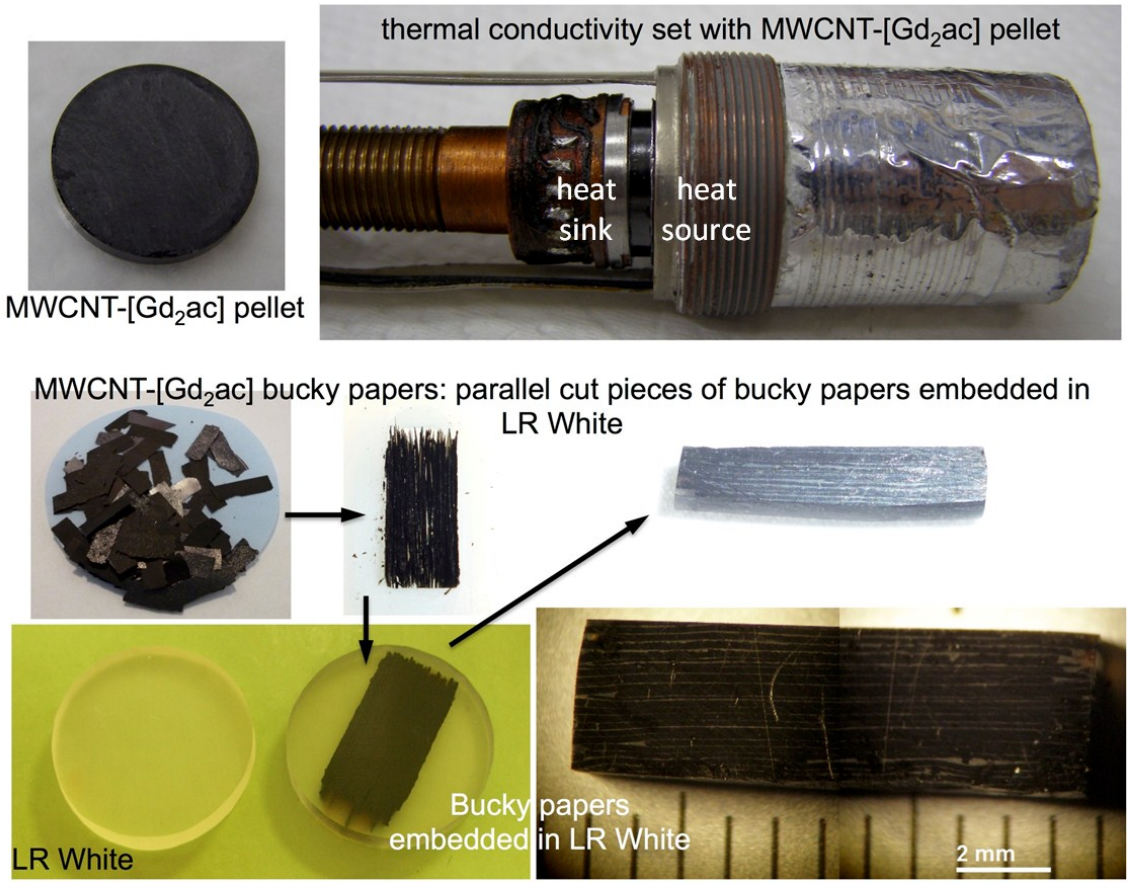

Figure S15. Details of the setup used for thermal conductance measurements and samples used for these measurements.

Table S2. Dimensions, weights and derived apparent densities of the four samples used for the thermal conductivity study.

Sample	mass (g)	area (cm^2)	height (cm)	V (cm^3)	d_{app} (g/cm^3)
[Gd_2ac] pellet	1.10720	1.379	0.445	0.6136	1.804
MWCNT-[Gd_2ac] pellet	0.36666	1.379	0.165	0.2275	1.612
MWCNT-[Gd_2ac] in LR White	0.11495	0.3873	0.225	0.08715	1.319
LRWhite	0.49864	1.735	0.2575	0.4467	1.116

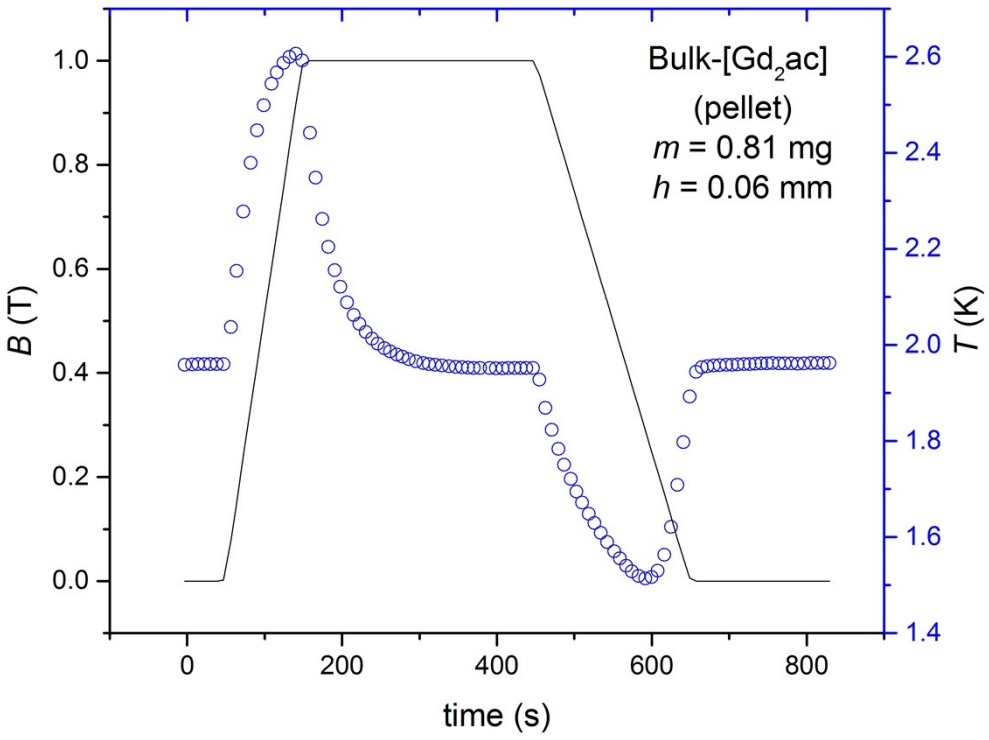

Figure S16. Direct measurement of the magnetocaloric effect for a pellet sample of bulk-[Gd_2ac] (m = 0.81 mg). Line: time evolution of the applied field B ($0 \rightarrow 1$ T $\rightarrow 0$); points: experimental temperature T, as labeled, starting from T = 1.96 K.

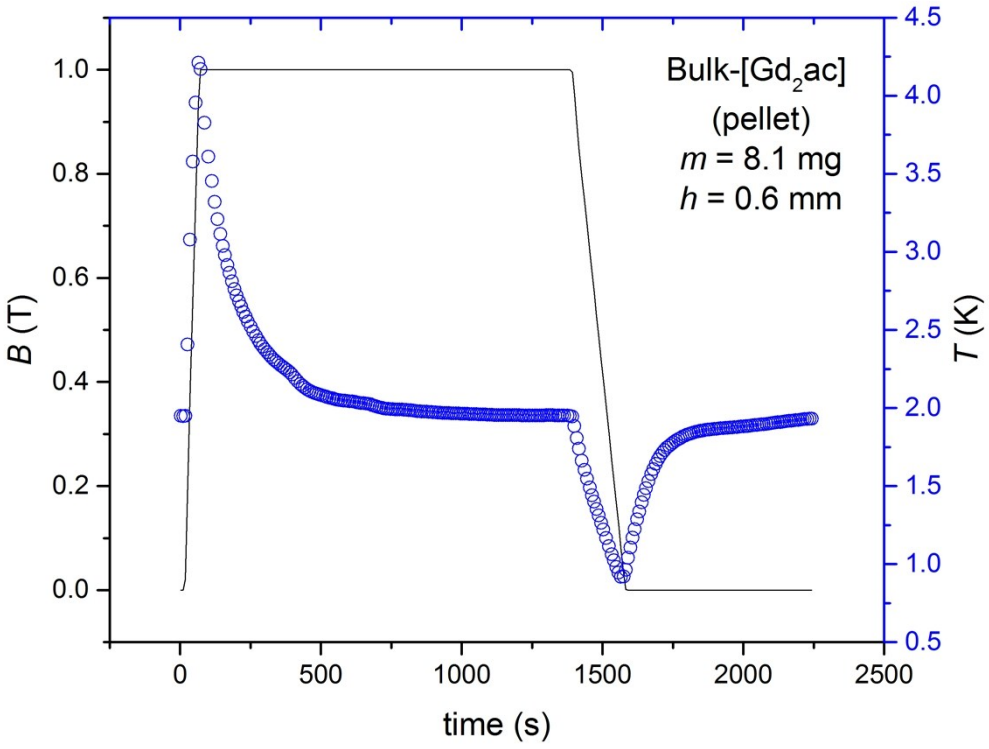

Figure S17. Direct measurement of the magnetocaloric effect for a pellet sample of bulk-[Gd_2ac] (m = 8.1 mg). Line: time evolution of the applied field B ($0 \rightarrow 1$ T $\rightarrow 0$); points: experimental temperature T, as labeled, starting from T = 1.96 K.

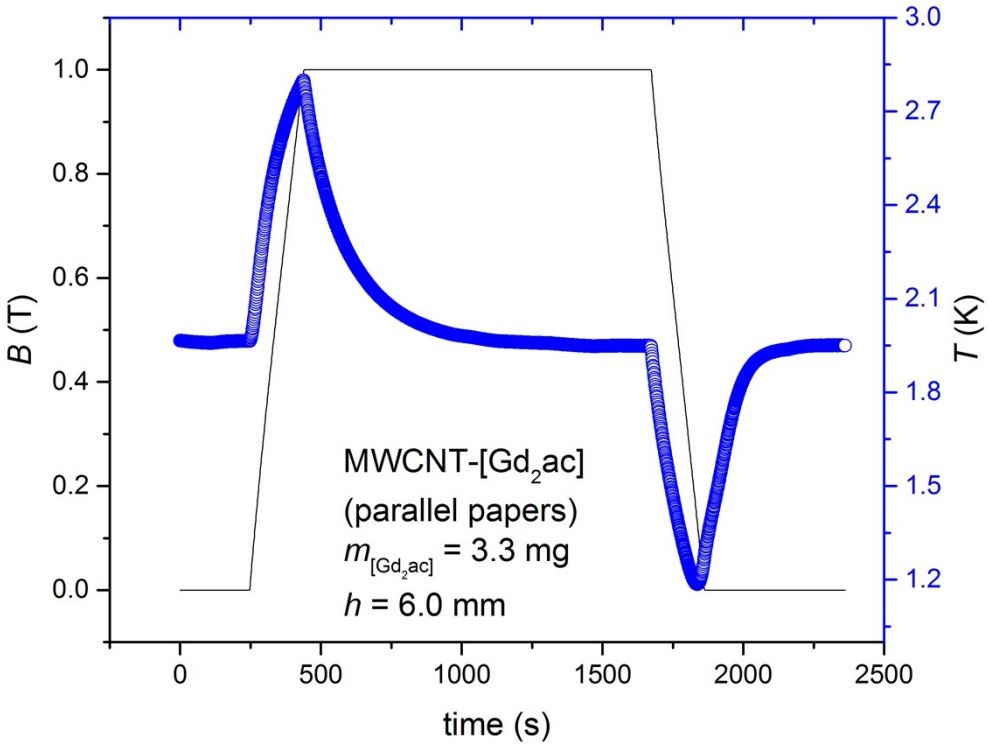

Figure S18. Direct measurement of the magnetocaloric effect for an array of parallel buckypapers of MWCNT-[Gd_2ac] ($m_{[Gd2ac]}$ = 3.3 mg, normalized per [Gd_2ac]). Line: time evolution of the applied field B (0 $\rightarrow$ 1 T $\rightarrow$ 0); points: experimental temperature T, as labeled, starting from T = 1.96 K.

Modelling of the intrinsic thermal conductivity and direct MCE measurements

In our experiments, the cylindrically-shaped sample of bulk-[Gd_2ac] lies on top of a sapphire platform (see scheme below), which is mechanically suspended and thermally connected to a thermal bath, hold at constant temperature T_0, by wires of known thermal conductance $K_w(T)$. At liquid-helium temperatures, platform, thermometer and wires contribute negligibly to the heat capacity, which is then entirely determined by the sample. We assume that the temperature of the sample (a) is homogenous along any direction parallel to the sapphire platform, (b) has a gradient along z, *i.e.*, the direction perpendicular to the sapphire platform.

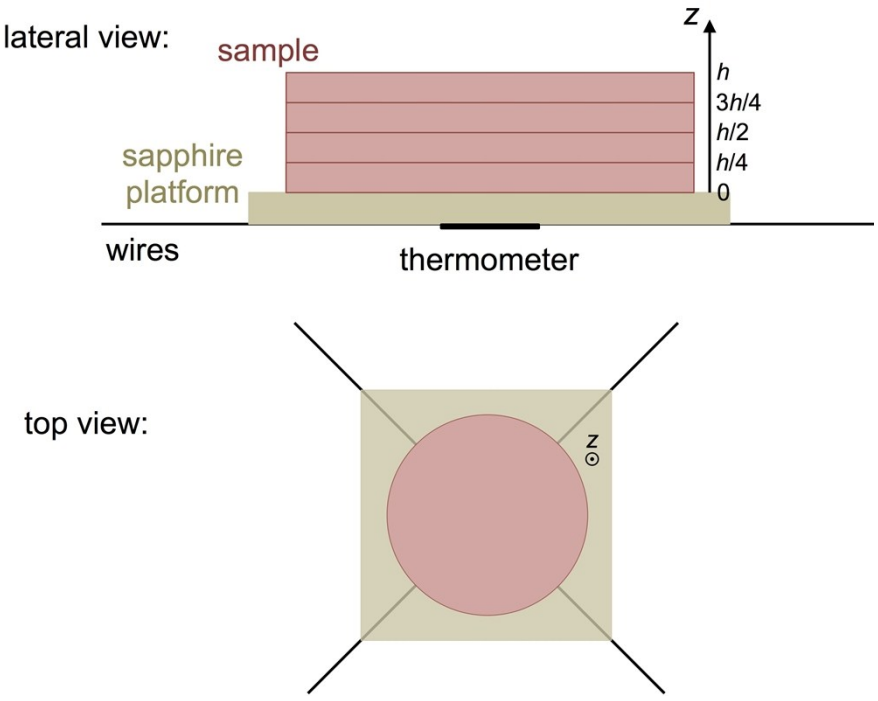

For any time-instant t in which the applied magnetic field B varies continuously, we simulate the evolution of the temperature, $T(t,z)$, across the

sample. Specifically, we discretize the height, h, of the sample into 32 sections and calculate the temperature for each section, although only the following values of the heights are recorded as representative ones, namely $z = 0$ (*i.e.*, in contact with the platform), $h/4$, $h/2$, $3h/4$ and h. All relevant parameters are considered as data inputs in our simulation.

Next, we derive the equation which describes the heat conduction. Let us consider one mass unit of magnetocaloric material in the bore of a superconducting coil, which produces a magnetic field B. The work done by an external source to hold a current in the superconducting coil is $dW = BdM$. Therefore, any infinitesimal change in energy can be expressed as $dU = dQ + dW = dQ + BdM$, according to the first law of thermodynamics. Let us further consider the magnetic enthalpy of a solid magnetic system when the pressure is negligible, *i.e.*, $H = U - MB.$ For any infinitesimal change, we thus obtain:

$$dH = dU - MdB - BdM = dQ - MdB = TdS - MdB. \tag{1}$$

Note that dH can also be written in terms of dT and dB, *i.e.*,

$$\begin{aligned} dH &= \left(\frac{\partial H}{\partial T}\right)_B dT + \left(\frac{\partial H}{\partial B}\right)_T dB = c_p dT + \left(\frac{TdS - MdB}{dB}\right)_T dB \\ &= c_p dT + T\left(\frac{\partial S}{\partial B}\right)_T dB - MdB, \end{aligned} \tag{2}$$

where c_p is the heat capacity of the sample under constant applied magnetic field. By equating (1) to (2), we obtain:

$$dQ = c_p dT + T\left(\frac{\partial S}{\partial B}\right)_T dB. \tag{3}$$

The heat gained through conduction by any volume V of the magnetocaloric material in an infinitesimal time interval dt is given by

$$\begin{aligned} dQ &= -dt\oint_A \mathbf{J}_Q \cdot d\mathbf{A} = dt\oint_A \kappa\nabla T \cdot d\mathbf{A} = dt\int_V \nabla\cdot\left(\kappa\nabla T\right)dV \\ &= dt\int_V \left(\nabla\kappa\cdot\nabla T + \kappa\nabla^2 T\right)dV, \end{aligned} \tag{4}$$

where J_Q is the heat flux density, A is the surface enclosing V, and κ is the intrinsic thermal conductivity of the sample. In (4) we make use of the Fourier law and the divergence theorem. The intrinsic thermal conductivity is included in our simulations by fitting the experimental data in Figure 4 to a $\kappa = \alpha T^n$ dependence at low temperatures. The gradient $\nabla\kappa$ can then be expressed as

$$\nabla\kappa = \frac{d\kappa}{dT}\nabla T = n\alpha T^{n-1}\nabla T = \frac{n\kappa}{T}\nabla T.$$

Moreover, for any small volume V the integrand in (4) can be considered constant and this equation simplifies to

$$dQ = Vdt\left[\frac{n\kappa}{T}\left(\nabla T\right)^2 + \kappa\nabla^2 T\right].$$

Replacing dQ in (3), for mass ρV, where ρ is the density, we obtain:

$$\kappa V dt\left[\frac{n}{T}\left(\nabla T\right)^2 + \nabla^2 T\right] = \rho V c_p dT + \rho V T\left(\frac{\partial S}{\partial B}\right)_T dB$$

or, equivalently,

$$dT = \frac{\kappa dt}{\rho c_p}\left[\frac{n}{T}\left(\nabla T\right)^2 + \nabla^2 T\right] - \frac{T}{c_p}\left(\frac{\partial S}{\partial B}\right)_T dB. \tag{5}$$

This is the master equation commonly employed for the simulation of heat transfer in prototypes of magnetocaloric refrigerators.[3] The last term in (5) can be transformed using the exact thermodynamic relation

$$-\frac{T}{c_p}\left(\frac{\partial S}{\partial B}\right)_T = \left(\frac{\partial T}{\partial B}\right)_S,$$

thus, yielding:

$$dT = \frac{dt}{\rho c_p}\left[\frac{n\kappa}{T}(\nabla T)^2 + \kappa\nabla^2 T\right] + \left(\frac{\partial T}{\partial B}\right)_S dB. \qquad (6)$$

Finally, dividing each term by dt and considering that, in one dimension, the temperature $T(t,z)$ is a function of time t and of a single space coordinate z, we obtain:

$$\frac{\partial T}{\partial t} = \frac{\kappa}{\rho c_p}\left[\frac{n}{T}\left(\frac{\partial T}{\partial z}\right)^2 + \left(\frac{\partial^2 T}{\partial z^2}\right)\right] + \left(\frac{\partial T}{\partial B}\right)_S \frac{dB}{dt}. \qquad (7)$$

Note that $\left(\frac{\partial T}{\partial B}\right)_S$ is relatively simple to implement in a numerical calculation, thus minimizing discretization errors. For instance in the present case, we deal with a nearly paramagnetic material, for which $\left(\frac{\partial T}{\partial B}\right)_S \cong \frac{T}{B}$. Equation (7) is finally solved numerically by using the Crank-Nicolson method.[4]

Furthermore, we determine the adiabatic temperature T_{ad}, *viz.*, the temperature if the sample would have been kept thermally isolated, using the same method we employed for other works.[5] Briefly, we note that the non-adiabaticity induces a variation of the entropy $\Delta S = S(t) - S(t_0)$ in a time interval $t - t_0$, which can be

---

[3] See, *e.g.*, K. K. Nielsen, J. Tusek, K. Engelbrecht, S. Schopfer, A. Kitanovski, C. R. H. Bahl, A. Smith, N. Pryds, A. Poredos, *Int. J. Refrig.* **2011**, 34 603-616

[4] J. Crank, P. Nicolson, *Proc. Camb. Phil. Soc.* **1947**, 43, 50-67

[5] See, *e.g.*, J. W. Sharples, D. Collison, E. J. L. McInnes, J. Schnack, E. Palacios, M. Evangelisti, *Nat. Commun.* **2014**, 5, 5321

expressed as $\Delta S = \int_{t_0}^{t} K_w (T_0 - T)/T dt$ at every time instant. We also have $\Delta S = \int_{T_{ad}}^{T} c_p(T, B)/T dT$, where the adiabatic temperature T_{ad} is the only unknown and can therefore be deduced numerically.

The results of the simulation are compared with the experimental temperatures collected for two pellet samples of bulk-[Gd_2ac] with a spherical-shaped base, $h = 0.06$ and 0.6 mm, respectively (Figures 5 and 6), and for an array of parallel buckypapers of MWCNT-[Gd_2ac] with rectangular-shaped base and $h = 6.0$ mm (Figure 6).